Methods

Homology modeling of the LMAN1 structure

The human LMAN1 structure was built through homology modeling by using the known structure of rat CRD of LMAN1 (PDB code: 1R1Z), which shares a sequence identity of 95% (sequence similarity 99%), as a template. The first 12 residues, which have been shown to have no impact for LMAN1-MCFD2 interactions in co-IP experiments (ΔN), were knocked out in homology modeling. Sixty models (**S1**) were generated and fully refined through high-level optimization by Modeller9V7[1]. Among them, the one with the lowest probability density function (PDF) energy was chosen for the final human LMAN1 model.

The RAMPAGE[2] program was applied to check the stereo chemical quality of this model. The Ramachandran plot (**S2**) produced by RAMPAGE shows that 98.2% of residues in our model are in the most favored regions, 1.8% of residues are in generally allowed regions, and there are no residues in outliner regions. These results indicate that the model of LMAN1 is good statistically.

Molecular docking of LMAN1 and MCFD2

The NMR structure of human MCFD2 (PDB code: 2VRG) and the modeled structure of the CRD of human LMAN1 were employed to produce a docking model of the LMAN1-MCFD2 complex. Initially 2000 LMAN1-MCFD2 complex models (**S3**) were generated by ZDOCK[3]. All the parameters were set as described in the previous report[4]. ZRANK[5] scoring function was applied to rerank the initial LMAN1-MCFD2 poses that were built by ZDOCK, and the one with the lowest ZRANK score was chosen as the model of the LMAN1 (CRD)-MCFD2 complex.

Refinement of the LMAN1-MCFD2 complex

Models generated by ZDOCK usually contain atom clashes at the interface of two proteins and energy minimization is a necessary step for final models. Thus, SPBDV[6] was employed for this purpose. The model comes from ZDOCK suffered 500 steps of steepest descent and 500 steps of conjugate gradients minimizations both of which applied for bond length, bond angles, bond torsions, non-bonded length, electrostatic and improper angles. Other key parameters used in energy minimization included: Lock/Constrain is for Carbon Alpha only; use a harmonic constrain; stop when delta E between two steps is below 0.02 KJ/mol.

Results and Discussion

The model of the CRD of human LMAN1

The overall modeled structure of human CRD is nearly identical to the rat structure **(Fig. S1A),** owing to the high sequence homology between them. Both D181A and

N156A abolish mannose binding. In the calcium binding region **(Fig. S1B)**, D181 forms two salt bridges with both calcium cations with distances of 2.4Å and 2.6Å respectively. N156 also interacts with one of the calcium cations by a salt bridge with a distance of 2.4 Å. Mannose binding site is adjacent to this calcium binding region[7]. Mutating D181 or N156, would probably lead to the conformational changes of the whole calcium binding region and disrupt mannose binding.

LMAN1-MCFD2 Complex Model

From the docked complex structure (**Fig. S2A)**, LMAN1 and MCFD2 interact through an interface of 805.6 $Å^2$. Their interactions mainly occur between the N-terminus of LMAN1 and the EF-hand region of MCFD2. Detailed contacts in the LMAN1-MCFD2 complex were analyzed by PROTORP[8] as shown in **Table S1**.

Two hydrogen networks were found between LMAN1 and MCFD2: one is K49(LMAN1)-N119(MCFD2)-R122(MCFD2) which consists of two hydrogen bonds; the other one is Y48(LMAN1)-R122(MCFD2) which contains two strong hydrogen bonds and the distance for both of which are 2.7 Å. Moreover, the stabilization of Y48(LMAN1)-R122(MCFD2) network is further enhanced by CH- π stack between Y48(LMAN1)-L125(MCFD2)(**Fig. S2B**). There are two additional strong interactions between LMAN1 and MCFD2: one is a strong hydrogen bond between K53(LMAN1) and D89(MCFD2); the other one is a salt bridge between H56(LMAN1) and H80(MCFD2), which is forward straightened by π - π stack between H56(LMAN1)- Y82(MCFD2) (**Fig. S2B**).

During the preparation of this manuscript, the crystal structure of LMAN1-MCFD2 complex (PDB Code: 3A4U) was released in the PDB Bank. Our model is very similar to the x-ray crystal structure at the binding area. However, there are also some differences between the model and X-ray structure, noticeably, some shifts occurred for three helixes in MCFD2 upon binding to the CRD.

1. A. Šali and T. L. Blundell. Comparative protein modelling by satisfaction of spatial restraints. J. Mol. Biol. 1993;**234**, 779-815.
2. S.C. Lovell, I.W. Davis, W.B. Arendall III, P.I.W. de Bakker, J.M. Word, M.G. Prisant, J.S. Richardson & D.C. Richardson. Structure validation by Cα geometry: φ/ψ and Cβ deviation. Proteins: Structure, Function & Genetics. 2002; **50**: 437-450.
3. Chen R, Li L, Weng Z. ZDOCK: An Initial-stage Protein Docking Algorithm. Proteins 2003; **52**, 80-87.
4. Wiehe K, Pierce B, Tong W, Hwang H, Mintseris J, Weng Z The Performance of ZDOCK and ZRANK in Rounds 6-11 of CAPRI. Proteins, 2007;**69**(4), 719-725.
5. Brian Pierce and ZhipingWeng*. ZRANK: Reranking Protein Docking Predictions With an Optimized Energy Function. PROTEINS: Structure, Function,

and Bioinformatics 2007;**67**:1078–1086

6. Guex, N. and Peitsch, M.C. SWISS-MODEL and the Swiss-PdbViewer: An environment for comparative protein modeling. Electrophoresis 1997;**18**, 2714-2723
7. Velloso, L.M.,Svensson, K.,Pettersson, R.F.,Lindqvist, Y. The Crystal Structure of the Carbohydrate-recognition Domain of the Glycoprotein Sorting Receptor p58/ERGIC-53 Reveals an Unpredicted Metal-binding Site and Conformational Changes Associated with Calcium Ion Binding. J. Mol. Biol. 2003;**334**, 845-851
8. Reynolds C, Damerell D, Jones S. ProtorP: a protein-protein interaction analysis server. Bioinformatics. 2009 Feb 1; **25**(3):413-4.
9. DeLano, W.L. The PyMOL Molecular Graphics System (2002) on World Wide Web http://www.pymol.org

Figure S1. Homology modeling of human LMAN1

(A) The overall modeled structure of human CRD is nearly identical to the rat structure. (B) Details of the calcium binding region.

Figure S2. Docking model of the LMAN1 (CRD)-MCFD2 complex

(A) Overview of the docked structure of the CRD-MCFD2 complex. (B) Two hydrogen networks between LMAN1 (yellow) and MCFD2 (blue).

Figure S3. Oligomerization analysis of LMAN1 mutants by reduced SDS-PAGE

COS1 cells were transfected with indicated wild type or LMAN1 mutants. Cells were lysed with the NP-40 buffer and mixed with the SDS loading buffer without reducing agent. LMAN1 species were resolved by SDS-PAGE and detected by a monoclonal anti-Flag antibody.

Figure S4. Diagram of BiFC constructs used in the experiments

Figure S5. BiFC images of MCFD2 fusion and various LMAN1 mutant fusions in HeLa cells

Hela cells were grown in six-well plates and transfected with 0.25μg of each indicated plasmid. Ten hours after transfection, fluorescent signals were observed under an inverted fluorescence microscope.

Figure S6. Oligomerization analysis of LMAN1 mutants using BiFC assay in living cells

(A) BiFC signals observed under fluorescent microscope. (B) Western-blot shows expression levels of the indicated fusion proteins. (C) Quantitative analysis of BiFC signals. Statistical analysis was performed using student's *t*-test and the asterisks indicate significant differences ($p<0.05$).

Table S1. Summary of effects of LMAN1 mutants used in the study

LMAN1 mutants	Effects on MCFD2 binding, mannose binding, ER exit and oligomerization	Effects on FV/FVIII binding
ΔCRD	No binding to MCFD2	No binding to FV/FVIII
ΔHelix	Binds MCFD2	Binds FV/FVIII
ΔHM	Monomer, bind mannose but does not bind MCFD2	Binds FVIII
C466A/C475A	Disulfide mutations, normal ER exit	N/A
N156A	Binds MCFD2, disrupts mannose binding	No binding to FV/FVIII
D181A	Binds MCFD2, disrupts mannose binding	No binding to FV/FVIII
KKAA	ER exit deficient, hexamer	N/A
ΔN	Binds MCFD2	N/A
Y48A	Binds mannose but does not bind MCFD2	Binds FVIII
K53A	Binds MCFD2	N/A
Y48A/K53A	No binding to MCFD2	N/A
W67S	Disrupt mannose binding and MCFD2 binding	N/A
Δβ1	Binds mannose but does not bind MCFD2	Binds FVIII
Δβ2	Disrupt mannose binding and MCFD2 binding	N/A
Δβ3	Disrupt mannose binding and MCFD2 binding	N/A
Δβ4	Disrupt mannose binding and MCFD2 binding	N/A

N/A, not analyzed.

Table S2. Interactions between LMAN1 and MCFD2 analyzed by PROTORP

Chain ID	Residue Number	Residue Name	Interface ASA	% Interface ASA	Segment	H-Bonds
A [1]	45	ARG	84.76	10.38	1	-
A	46	PHE	72.31	8.85	1	-
A	47	GLU	3.00	0.37	1	-
A	48	TYR	123.38	15.11	1	1
A	49	LYS	64.51	7.90	1	1
A	50	TYR	6.97	0.85	1	-
A	51	SER	9.90	1.21	1	-
A	52	PHE	8.52	1.04	1	-
A	53	LYS	69.48	8.51	1	-
A	55	PRO	52.27	6.40	1	-
A	56	HIS	65.94	8.07	1	1
A	57	LEU	5.20	0.64	1	-
A	59	GLN	33.53	4.11	1	-
A	65	PRO	41.03	5.02	2	-
A	66	PHE	83.88	10.27	2	-
A	96	LYS	48.45	5.93	3	-
A	97	THR	30.99	3.79	3	-
A	101	PHE	11.04	1.35	3	-
A	265	PHE	1.58	0.19	4	-
B [2]	80	HIS	56.90	6.97	4	1
B	82	TYR	89.50	10.96	4	-
B	83	ASP	15.22	1.86	4	-
B	89	ASP	27.95	3.42	5	-
B	90	GLY	26.63	3.26	5	-
B	91	LEU	125.74	15.40	5	-
B	92	GLU	5.26	0.64	5	-
B	94	SER	47.08	5.76	5	-
B	95	THR	31.25	3.83	5	-
B	114	GLU	12.95	1.59	6	-
B	115	ASP	40.61	4.97	6	-
B	118	ILE	83.28	10.20	6	-
B	119	ASN	19.86	2.43	6	-
B	121	ILE	13.66	1.67	6	-
B	122	ASP	38.60	4.73	6	2
B	125	LEU	29.85	3.65	6	-
B	126	ARG	83.91	10.27	6	-
B	132	ASN	18.46	2.26	7	-
B	133	ASP	10.68	1.31	7	-
B	134	GLY	29.66	3.63	7	-
B	135	TYR	27.52	3.37	7	-

1. ChainA is LMAN1
2. ChainB is MCFD2

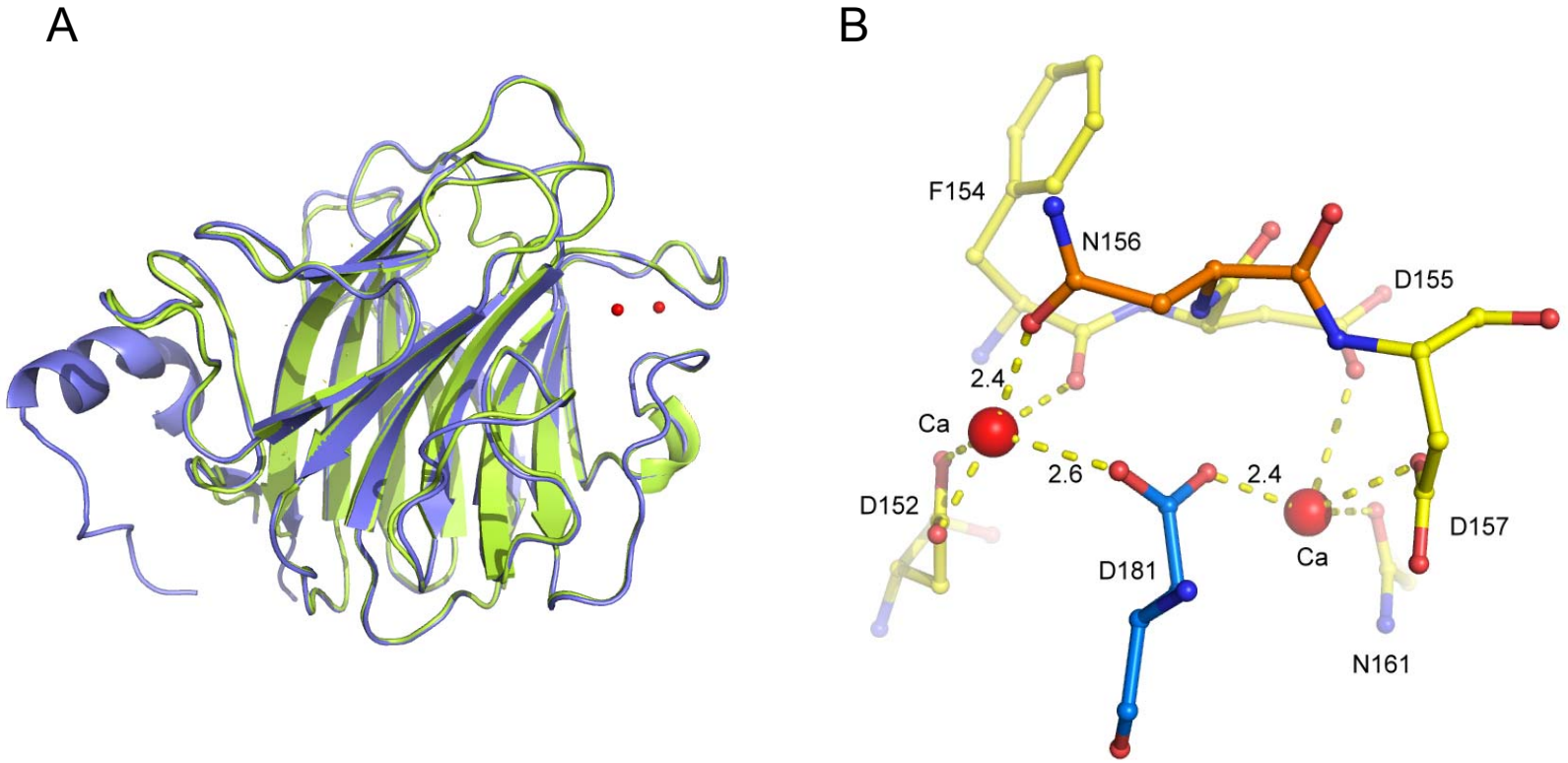

Figure S1

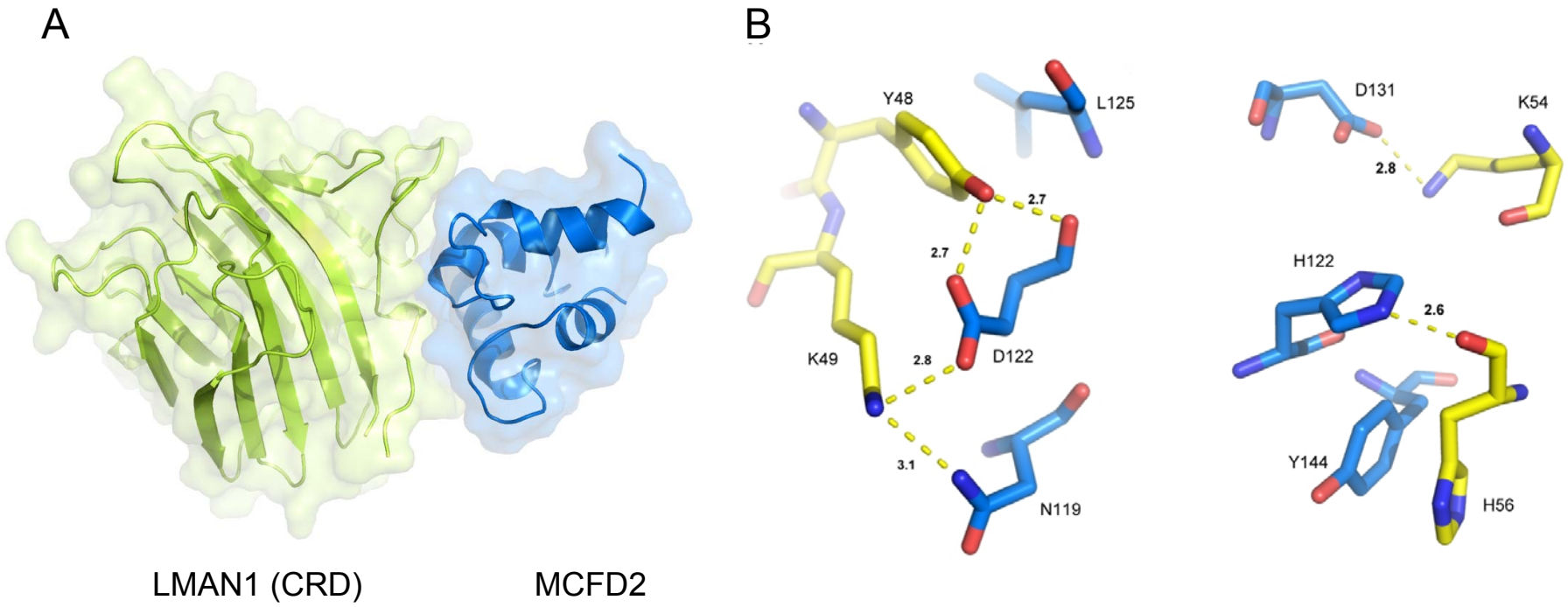
A
B
LMAN1 (CRD)
MCFD2
Y48
L125
2.7
2.7
K49
2.8
D122
3.1
N119
D131
K54
2.8
H122
2.6
Y144
H56

Figure S2

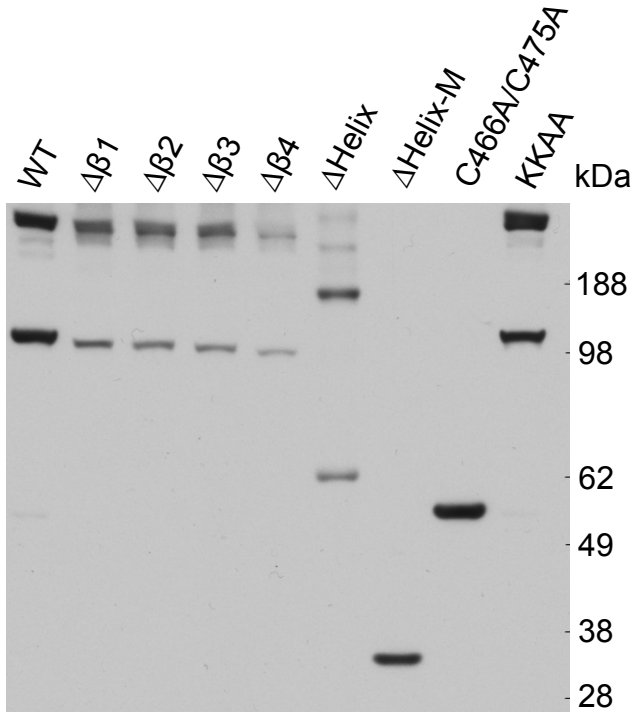
WT
Δβ1
Δβ2
Δβ3
Δβ4
ΔHelix
ΔHelix-M
C466A/C475A
KKAA
kDa
188
98
62
49
38
28

Figure S3

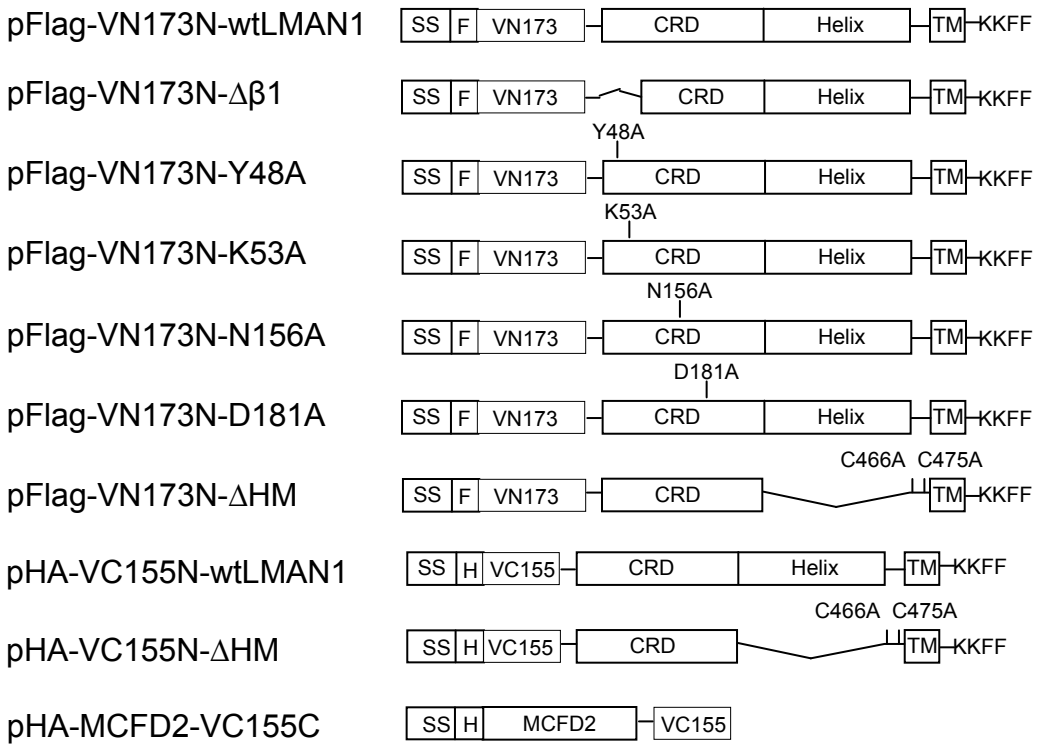
pFlag-VN173N-wtLMAN1
SS
F
VN173
CRD
Helix
TM
KKFF
pFlag-VN173N-Δβ1
pFlag-VN173N-Y48A
Y48A
pFlag-VN173N-K53A
K53A
pFlag-VN173N-N156A
N156A
pFlag-VN173N-D181A
D181A
pFlag-VN173N-ΔHM
C466A
C475A
pHA-VC155N-wtLMAN1
H
VC155
pHA-VC155N-ΔHM
pHA-MCFD2-VC155C
MCFD2

Figure S4

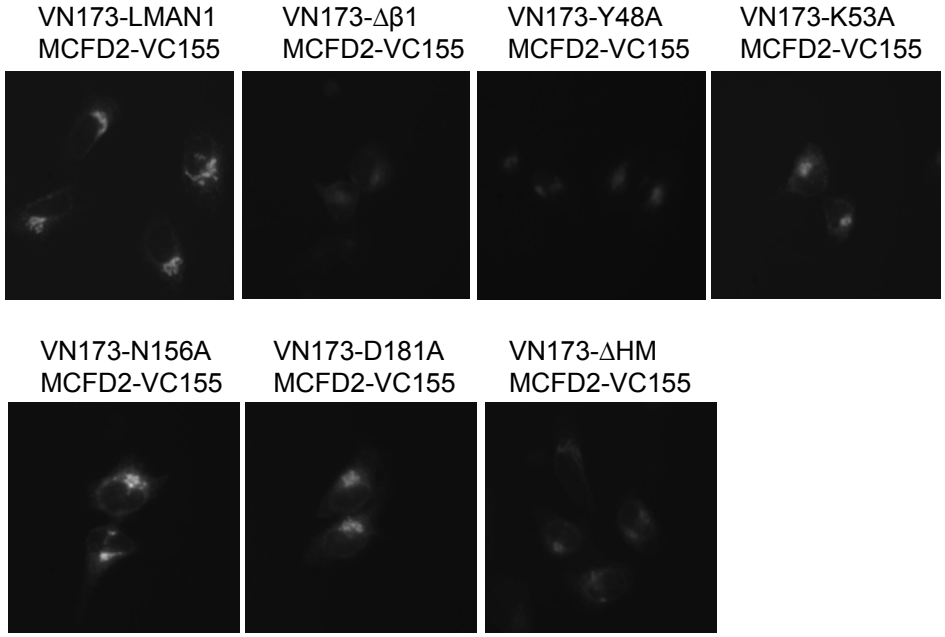
VN173-LMAN1
MCFD2-VC155
VN173-Δβ1
MCFD2-VC155
VN173-Y48A
MCFD2-VC155
VN173-K53A
MCFD2-VC155
VN173-N156A
MCFD2-VC155
VN173-D181A
MCFD2-VC155
VN173-ΔHM
MCFD2-VC155

Figure S5

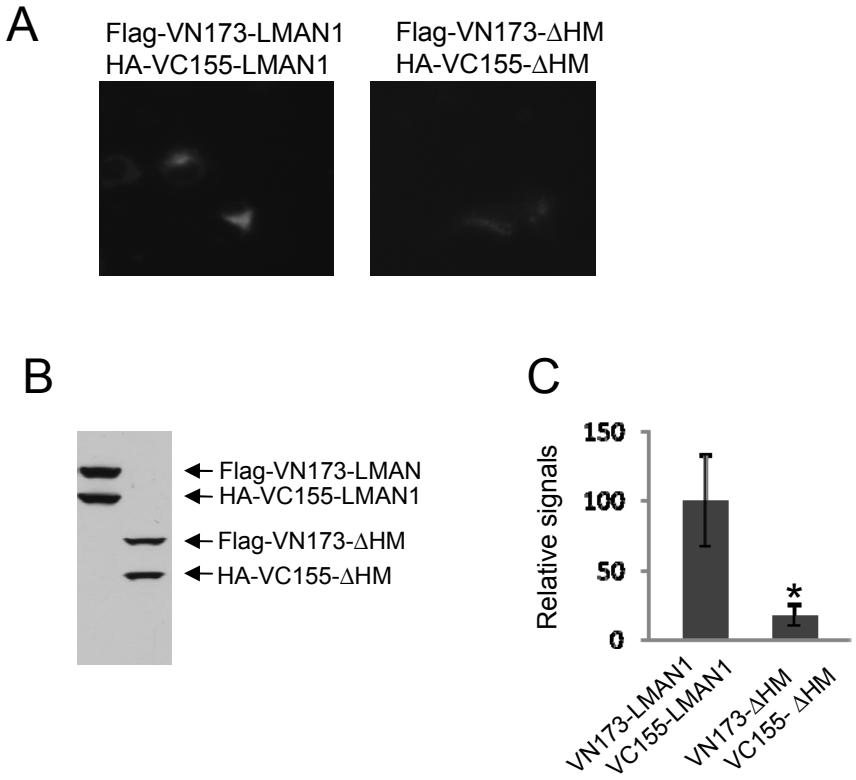
A
Flag-VN173-LMAN1
HA-VC155-LMAN1
Flag-VN173-ΔHM
HA-VC155-ΔHM
B
Flag-VN173-LMAN
HA-VC155-LMAN1
Flag-VN173-ΔHM
HA-VC155-ΔHM
C
Relative signals
150
100
50
0
*
VN173-LMAN1
VC155-LMAN1
VN173-ΔHM
VC155- ΔHM

Figure S6